Estimation of PM Machine Efficiency Maps From Limited Experimental Data

Solmaz Kahourzade[1], Amin Mahmoudi SMIEEE[2], Wen L. Soong MIEEE[1], Nesimi Ertugrul MIEEE[1], and Gianmario Pellegrino SMIEEE[3]
[1]School of Electrical and Electronic Engineering, University of Adelaide, Australia
[2]College of Science and Engineering, Flinders University, Australia
[3]Politecnico di Torino, Corso Duca degli, Abruzzi 24, Torino, 10129 Italy

***Abstract*— This paper investigates the accuracy of the estimation of efficiency maps for permanent magnet (PM) machines using experimental measurements of stator resistance, back-emf and inductances, plus the iron loss versus speed characteristic. The approach is validated using detailed finite-element results for 50-kW surface and interior PM machines. The paper examines the effect on the torque-speed capability curve when modeling the flux-linkage characteristics using linear and saturating models. The modelling of the iron/magnet losses under maximum efficiency operation as a function of torque and speed is considered using the open-circuit, short-circuit and no-load iron/magnet losses. A novel approach based on scaling the no-load losses as a function of load is proposed and shown to give promising results.**

***Keywords*— Efficiency maps, loss modeling, no-load loss, permanent magnet machines.**

I. Introduction

Efficiency maps are commonly used to graphically illustrate and compare the performance of electric machines. They are contour plots of maximum efficiency on axes of torque (or power) versus speed. Efficiency maps show not only the capability envelope of the machine but also the efficiency at all possible operating points.

Efficiency maps for electrical machines can be obtained experimentally but this requires the availability of sophisticated and accurate test equipment. They can also be estimated using either detailed finite element (FE) simulations or using the *d-q* equivalent circuit. An accurate calculation of the efficiency maps for electrical machines relies on detailed flux linkage and loss determination. FE analysis is considered the most precise method to calculate the efficiency map that considers the machine's non-linearities as well as hysteresis and eddy-current losses [1]. It requires significant post-processing which includes loss data analysis for each torque-speed point in the T-ω plane.

The alternative method is analytical calculation based on the equivalent circuit parameters (obtained either experimentally or from FE simulations). It uses the simplified loss model which mostly considers the non-copper loss as a function of speed only [2, 3]. These simplifying assumptions result in a coarse estimation of efficiency map which can be improved by considering the impacts of saturation and cross coupling [4]. It has been shown in [5] that estimating the non-copper loss only as a function of speed results in large error especially in the field weakening region.

This paper focusses on an important problem which has received limited attention in the literature: examining the accuracy of estimating efficiency maps using limited experimental tests. It improves the accuracy of the efficiency map estimation obtained from measured equivalent circuit parameters (including back-emf, inductances, stator resistance and losses) by proposing a novel loss scaling technique. This method is based on separate loss modelling, and scaling of the measured no-load losses in the constant torque and constant power regions.

To validate the approach, the proposed experimental method is checked using detailed FE analysis results on example 50-kW surface and interior PM machines. This approach allows comparison between the "exact" efficiency map predicted by using the detailed FE analysis results and the estimated efficiency map using the equivalent circuit parameters extracted from the same FE analysis data.

II. Theoretical Framework

The efficiency map shows the maximum machine efficiency at a given torque/speed point that satisfies the machine constraints including voltage limit (usually set by the power converter DC bus voltage) and current limit (usually set by the machine/inverter thermal limits) (see Fig. 1a). Brushless PM machines normally use *d*- and *q*-axis current control to achieve smooth torque control and fast dynamic response. For a given speed, all combinations of I_d and I_q which produce the required torque (see Fig. 1b) and are compatible with both voltage and current constraints are considered (see Fig. 1c). Among these, the I_d and I_q combination resulting in the highest efficiency (lowest loss) is chosen (see Fig. 1d) to produce a single point on the efficiency map.

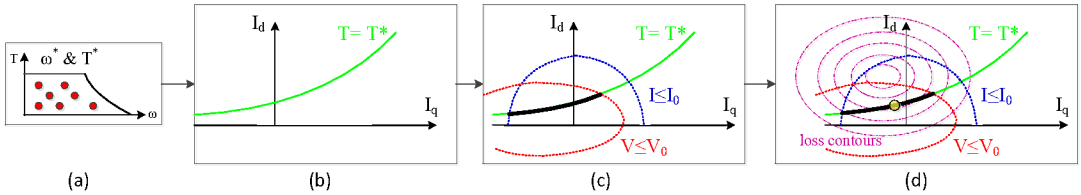

Fig. 1 Efficiency map calculation process.

A. Exact Efficiency Map from Detailed FE Analysis

The efficiency map of PM machines can be calculated by using FE analysis to obtain maps of the *d*- and *q*-axis flux-linkages and iron loss as a function of the *d*- and *q*-axis currents: $\lambda_d(I_d, I_q)$, $\lambda_q(I_d, I_q)$ and $P_{fe}(I_d, I_q)$ at a given speed [6]. It is also necessary to have the stator resistance R_s. For the flux-linkages, taking into account cross-saturation effects using $\lambda_d(I_d, I_q)$ and $\lambda_q(I_d, I_q)$ rather than the simpler saturation-only models, $\lambda_d(I_d)$ and $\lambda_q(I_q)$, allows improved accuracy for machines with high degrees of stator saturation.

The iron loss also includes the rotor magnet losses. The speed dependence is obtained by scaling the stator/rotor hysteresis and eddy-current loss terms separately $P_{fe}(I_d, I_q, \omega)$. It should be noted that the FE results do not include any mechanical (bearing friction and windage) losses. The net torque for a motor as a function of I_d, I_q and ω is found using,

$$T = \frac{mp}{2}\left[\lambda_d I_q - \lambda_q I_d\right] - \frac{P_{fe}}{\omega} \quad (1)$$

where m is the number of phases and p is the number of pole-pairs. The *d*- and *q*-axis voltages as a function of I_d and I_q are given by,

$$V_d = -\omega\lambda_q + I_d R_s \quad (2)$$

$$V_q = \omega\lambda_d + I_q R_s \quad (3)$$

The total loss as a function of I_d and I_q is given by the sum of the copper and iron losses,

$$P_{loss} = m\left(I_d^2 + I_q^2\right)R_s + P_{fe} \quad (4)$$

To determine the efficiency map, for each operating point defined as (T, ω), the value of (I_d, I_q) is found. This point produces the desired torque T at the desired speed ω from (1) while minimizing losses in (4) and not does exceed the rated current (I_0) or voltage (V_0),

$$\sqrt{I_d^2 + I_q^2} = I \le I_0 \quad \text{and} \quad \sqrt{V_d^2 + V_q^2} = \mathrm{V} \le V_0 \quad (5)$$

From these results the maximum efficiency as a function of (T, ω) can be found,

$$\eta = \frac{T\omega}{T\omega + P_{loss}} \quad (6)$$

This maximum efficiency for a given operating point is normally shown as a contour plot on the torque-speed plane and is called the efficiency map.

B. Experimental Parameter Measurements

Experimental measurements can be performed to obtain both the flux-linkage and the copper and iron loss parameters. For the flux-linkage, $\lambda_d(I_d, I_q)$ and $\lambda_q(I_d, I_q)$ can be obtained using rotating tests by controlling I_d and I_q with an inverter and measuring the resultant fundamental machine *d*- and *q*-axis voltages/flux-linkages.

It is often preferable to use simpler stationary tests of flux-linkage that can only provides $\lambda_d(I_d)$ and $\lambda_q(I_q)$ and these will be the results considered in this paper. A stationary test needs to be combined with an open-circuit test to obtain the back-emf and hence *d*-axis magnet flux-linkage $\lambda_d(I_d{=}0, I_q{=}0)$. A further approximation is to model the machine with constant values of *d*- and *q*-axis inductance L_d and L_q,

$$\lambda_d = \lambda_m + L_d I_d \quad \text{and} \quad \lambda_q = L_q I_q \quad (7)$$

The copper loss is determined by the stator resistance, R_s. The copper loss for a given operating point (T, ω) is sensitive to the accuracy of the flux-linkage characteristics as these determine the torque for a given (I_d, I_q) combination.

For the iron losses (and mechanical loss), it is possible to measure $P_{fe}(I_d, I_q, \omega)$ from rotating tests with an inverter and calculating the iron loss as the difference between the electrical input power and the mechanical output power after subtracting the stator copper losses. It is however often preferable to use simpler and quicker tests to measure the iron loss in different situations as a function of speed only. The three cases examined in this paper are two generating cases, open-circuit and short-circuit, and one motoring case, no-load.

For the generating tests, the machine is rotated using a drive machine and its iron (and mechanical) losses found as a function of speed under open and short-circuit conditions. The iron loss is given by the mechanical input power minus the stator copper loss which is found from the measured stator current (zero for the open-circuit test). In most PM machines, the short-circuit iron loss is higher than the open-circuit iron loss.

In this paper, the estimated open-circuit loss is found using the FE calculated $P_{fe}(I_d, I_q, \omega)$ with I_d and I_q both set to zero. For the estimated short-circuit loss, I_q is set to the negative characteristic current which is the high-speed short-circuit current. For the no-load test, the machine with no load on its shaft is driven by an inverter. It requires a small *q*-axis current to provide power for the iron (and mechanical) losses. At low speeds the *d*-axis current is zero, but at higher speeds, a negative value may be required to keep the terminal voltage below its rated value in (5). The no-load loss is determined from the electrical input power to the machine minus the stator copper losses. In this paper, the estimated no-load loss is found using the FE calculated $P_{fe}(I_d, I_q, \omega)$ with I_q set to zero, and I_d at the minimum negative value to satisfy the voltage constraint in (5) at each speed.

III. SPM and IPM Case Study

Two examples of 50-kW PM machines are considered in this paper, one an interior PM design (IPM) and the other a surface PM design (SPM) [7]. Both are designed for a traction application. Fig. 2 shows the cross-sections of the designs and Table I summarizes their parameters.

IV. Flux Linkage and Torque Estimation

Under real operating conditions, the electrical machines show some degree of saturation and cross-saturation. Under the cross-saturation condition (which is applicable to the most general case), the *d*- and *q*-axis flux linkages are functions of both *d*- and *q*-axis currents, $\lambda_q(I_d, I_q)$ and $\lambda_d(I_d, I_q)$. Fig. 3 (top rows) shows the *d*- and *q*-axis flux variation of the studied SPM and IPM machines as a function of the corresponding axis current, e.g. $\lambda_q(I_d)$. Due to cross-saturation, there are multiple values of flux-linkage associated with a given axis current (grey areas). This figures also shows the maximum efficiency region

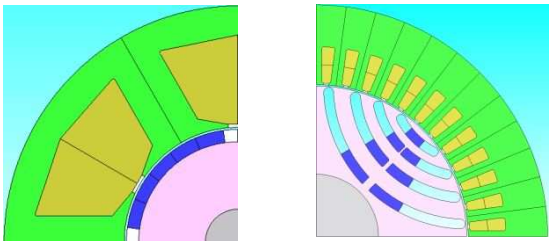

Fig. 2 Cross-sections of the two 50 kW machines (left SPM, right IPM).

TABLE I. Specifications of 50-kW, 12 kr/min Motors [7].

	IPM	SPM
Key Dimensions		
- stator outer diameter	216 mm	
- stack length	170 mm	
- airgap length	0.7 mm	1 mm
Design Parameters		
- poles	4	4
- stator slots	48	6
- number of turns	24	24
- copper slot fill (copper/slot area)	40%	55%
Electrical Parameters		
- torque @ 360 A	164 Nm	240 Nm
- characteristic current (peak)	210 A	240 A
- stator resistance @130°C	23 mΩ	20 mΩ

(yellow colour). These plots also shows the saturation-only model (red lines), and linear model (green lines). In the saturation and linear approximations, it is important that the flux in these regions is as close to the cross-saturation values as possible.

In general, the *d*-axis flux linkage magnitude decreases with increasing I_q current. The effect of cross saturation is more pronounced for the SPM compared to the IPM. This is likely because the *d*- and *q*-axis flux paths share more joint areas in the case of the SPM. The equivalent-circuit method is used to estimate the machine performance using the saturated and linear inductance models. When using a saturation-only model, the *d*- and *q*-axis flux linkages are assumed only functions of their respective current with the other current set to zero, that is $\lambda_d(I_d, I_q = 0)$ and $\lambda_q(I_d = 0, I_q)$.

With the highest level of approximation, the effect of saturation is ignored and machines are modeled with constant inductances ($\lambda_d = \lambda_m + L_d I_d$ and $\lambda_q = L_q I_q$, where L_d and L_q are constant). If the flux-linkages are not heavily saturated (like λ_q for SPM and λ_d for IPM), the linear model can provide acceptable estimation of the saturated results. For the IPM *q*-axis flux linkage, there are two possible estimates for the linear model. The first approximation (green line) represents the unsaturated inductance while the second model (green dashed line) illustrates an approximation of the saturated inductance.

The cross-saturation, saturation-only and linear flux-linkage models were used to predict the torque-speed capability curve in the right columns of Fig. 3. The SPM shows significant cross-saturation and so in the constant torque region ignoring this produces errors of up to 30%. For the IPM, the lower degree of cross-saturation means the saturation-only model shows good accuracy (about 4% error), but the both linear models have substantial errors.

In the constant power region, the machine operates with a constant voltage and a near constant current and thus the output power is much less sensitive to model flux-linkage errors. Thus all the models show relatively small errors in this region which reduce with increasing speed.

Fig. 4 shows the effect of the different flux linkage estimation models on the prediction of the copper loss in the torque-speed plane. For the SPM, it is difficult to compare the curves due to the substantial error in the capability curve in the

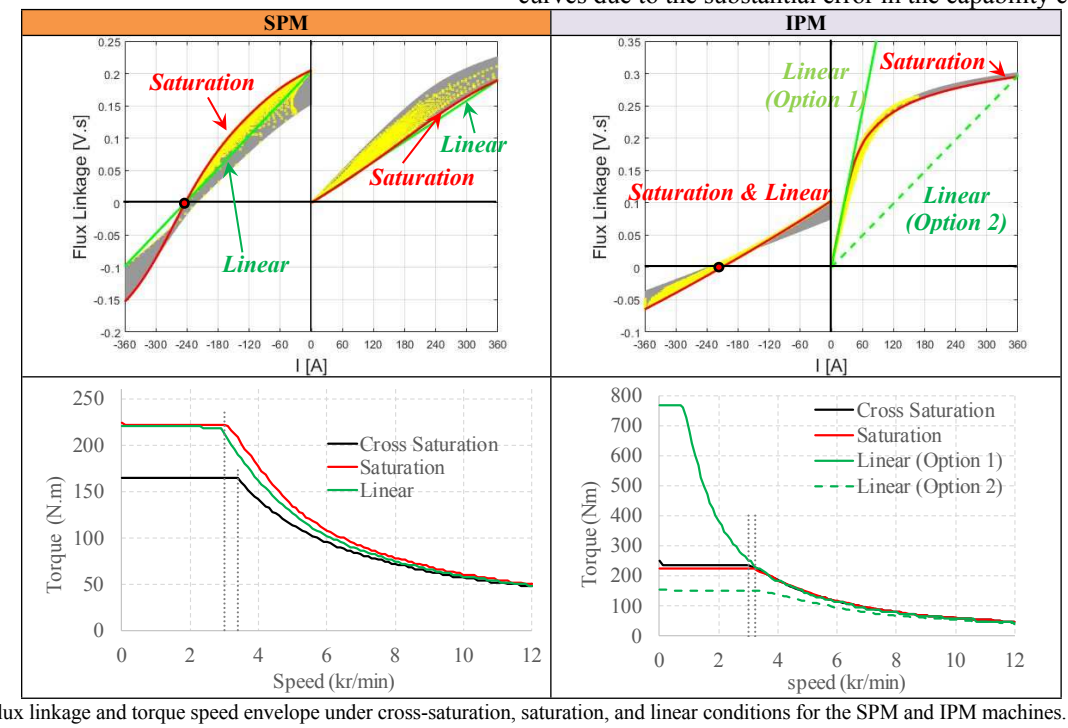

Fig. 3 Flux linkage and torque speed envelope under cross-saturation, saturation, and linear conditions for the SPM and IPM machines.

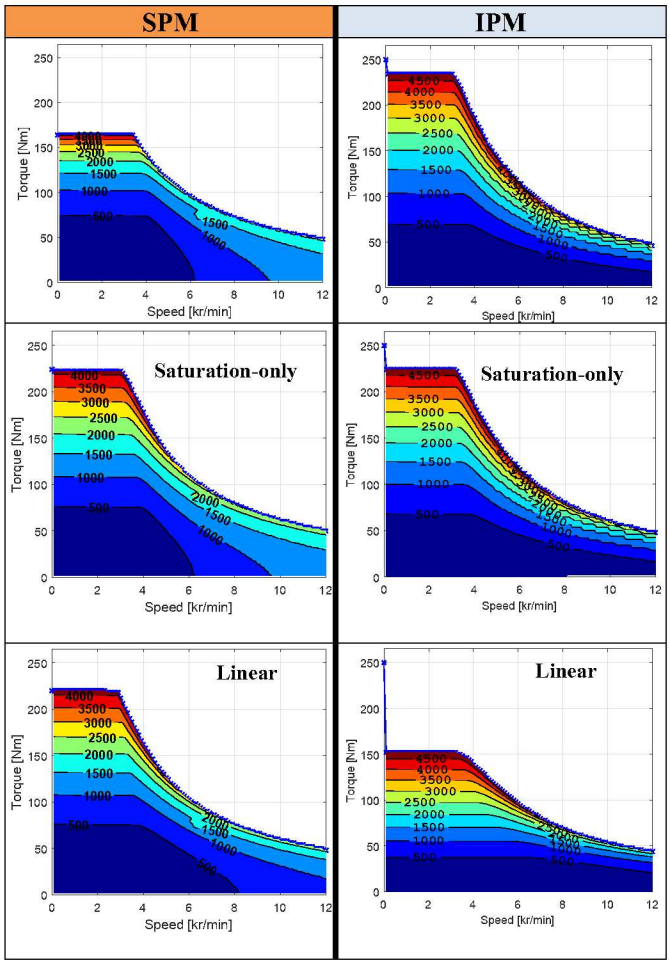

Fig. 4 Effect of flux-linkage estimation on copper loss. Actual and estimated copper loss values for the SPM and IPM motors (saturation-only and linear models).

constant torque region. The saturation-only model shows significantly better prediction than the linear model in the constant power region.

For the IPM, the saturation-only model shows good correspondence with the actual result. The presented linear model is based on second option shown in Fig.3. It illustrates a large error as expected from the inaccurate *d*-axis flux linkage.

V. Iron Loss Estimation

The efficiency map shows the maximum efficiency for each (T,ω) operating point in the torque-speed plane. Each operating point has a corresponding copper and iron losses and the sum of them is the total loss. Note that this study is based on FE results and so does not include mechanical losses.

Fig. 5 shows the total loss (blue points) and the iron loss only (green points) at maximum efficiency operation over the entire efficiency map plotted versus speed for both the SPM and IPM machines. Given these losses generally increase with load, the loss point for each speed with the lowest loss corresponding to no load and the highest loss point corresponding to full load. The open-circuit (OC), short-circuit

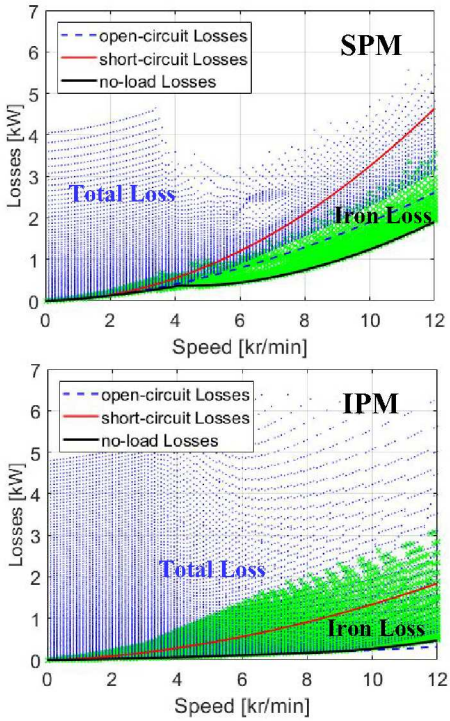

Fig. 5 Scatter plot of iron loss and total loss versus speed overlaid by the SC, OC, and NL losses versus speed curves (top SPM, bottom IPM).

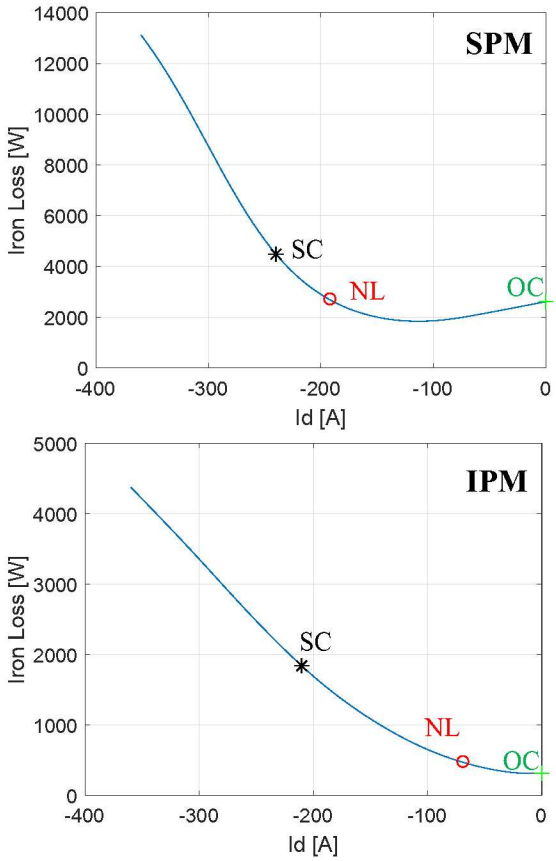

Fig. 6 Iron loss for the SPM and IPM machines as a function of *d*-axis current with zero *q*-axis current at 12,000rpm. The OC, NL and SC operating points are indicated.

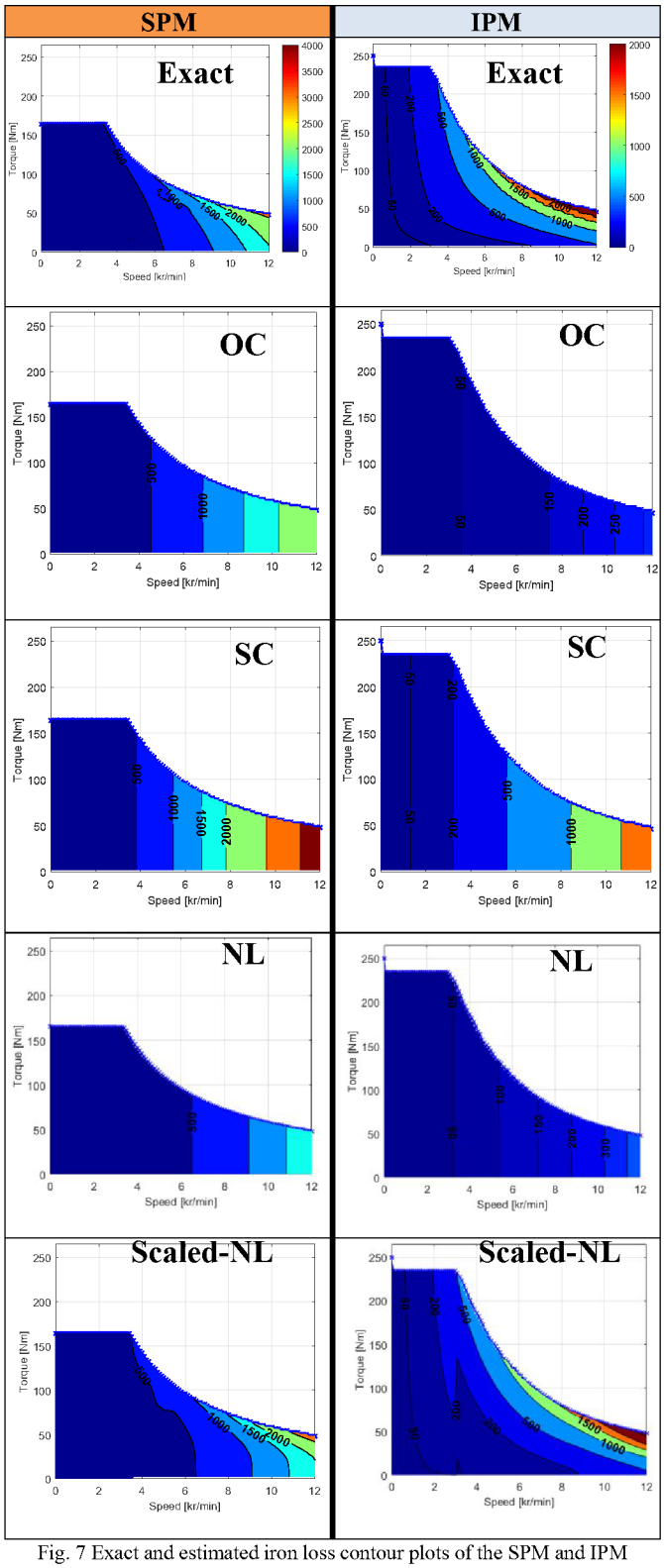

Fig. 7 Exact and estimated iron loss contour plots of the SPM and IPM motors.

(SC) and no-load (NL) iron losses as a function of speed are also included in these plots for comparison. Fig. 5 shows that for the considered two machines, the maximum iron loss (top envelope of green iron loss points) is significantly smaller than the maximum copper loss (largest difference between the highest blue and green points for the same speed). Copper loss is roughly related to the square of torque and iron loss is roughly related to the square of speed.

Fig. 6 shows that the NL loss in the field-weakening region for the SPM is less than the OC loss while the opposite is true for the IPM. This can be explained using Fig. 6 which illustrates the iron loss of these machines at the maximum speed of 12,000 rpm (field weakening region) as a function of d-axis current with zero q-axis current. The points corresponding to OC, NL and SC operation are indicated.

Increasing the magnitude of the d-axis current in PM machines has two effects. Firstly it reduces the fundamental flux density in the machine and hence the fundamental iron loss. Secondly it creates harmonic air-gap flux densities which produce harmonic iron losses.

For the SPM, the reduction in fundamental iron loss is initially greater than the increase in harmonic iron loss producing a minimum iron loss for a value of I_d of about -120A. This effect has been used earlier for loss minimization in SPM machines [8].

For the IPM machine, the iron loss increases monotonically with d-axis current indicating the increase in harmonic iron loss exceeds the reduction in fundamental iron loss.

The SC losses are generally larger than the OC losses and for the two machines are about two to three times larger. This is because the large negative d-axis currents required to bring the d-axis flux-linkage to zero, produce significant harmonic losses in the machine.

For the considered two machines, the average iron loss under load is best approximated by the OC loss for the SPM and the SC loss for the IPM. Fig. 7 shows the iron loss contour maps on axes of torque and speed and compares the exact case with estimates based on iron loss variation with speed only (OC, SC and NL). It also shows an improved approximation obtained by scaling the NL results with load which will be explained in the next section. A consistent contour scale for the results of each machine is used to allow comparison.

The differences in the iron loss are most evident in the constant power region where the losses are higher. The IPM shows a greater variation of iron loss with load than the SPM. As was observed from Fig. 7, the OC loss better approximates the average loss for the SPM while the SC loss is better for the IPM, however neither is particularly satisfactory at higher speeds.

VI. Modeling Iron Loss Variation with Load

The previous section showed that using the OC, SC, and NL loss results do not provide acceptable estimation of the iron loss as they don't model its variation with load. This is investigated in this section.

A. Loss Analysis According to the Operation Region

Fig. 8 shows plots of the iron loss at maximum efficiency along these lines of constant speed as a function of load, both

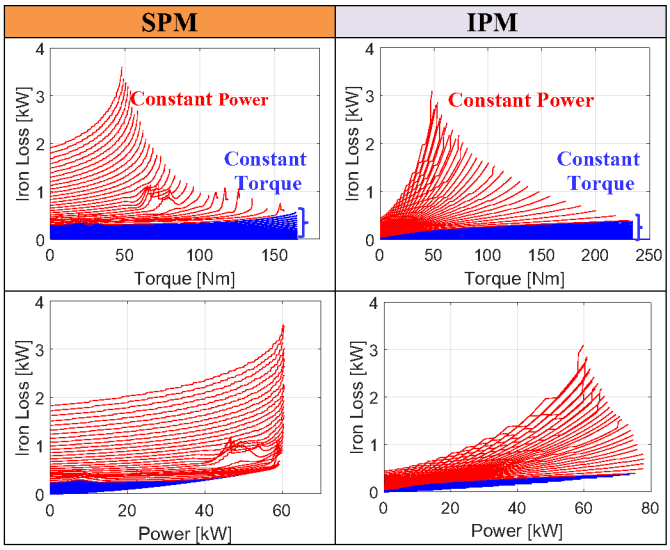

Fig. 8 Iron loss variation in the constant torque and constant power region versus torque and power.

torque (top graphs) and power (bottom graphs) for the SPM and IPM machines. Again the blue lines represent the constant torque region and the red lines the constant power region. As expected, in the curves plotted against load torque, the constant torque lines all have similar maximum torque and in the curves plotted against load power, the constant power lines have similar maximum power.

The loss at zero load corresponds to the NL iron loss and Fig. 8 shows that the iron loss increases smoothly with both load and speed. There is a minor irregularity in the SPM constant power curves at around 70Nm/50kW; this is likely to be due to numerical errors.

B. Normalizing the Iron Loss

By studying the results, in Fig. 8, it appears that within the constant torque and power regions, the curves for each speed have similar shape and may be scaled versions of one another. To test this, the curves for each speed are normalised by either the OC, SC and NL losses at the same speed and the results are shown in Fig. 9 for the SPM and IPM machines. In this figure, the first two rows are the results normalised by the OC losses as a function of load torque and power. The graphs in the next two rows are normalised by the SC losses and the final two rows are normalised by the NL losses.

The NL results were found to provide the best results. They had a unity ratio at no load and showed the best overall match for the constant torque and power region results for the two machines. The IPM constant torque curves had the closest match (smallest divergence), followed by the SPM constant torque and power curves, with the IPM constant power curves having the poorest match (largest divergence). It is interesting that the IPM constant power curves show similar shape for all three normalisations.

C. Finding Correct Function for Scaling the NL losses

It is proposed to represent the iron loss variations with load using a power law $y(x) = x^n$. Fig. 10 shows graphs with different guesses for the exponent n. For instance in the constant torque

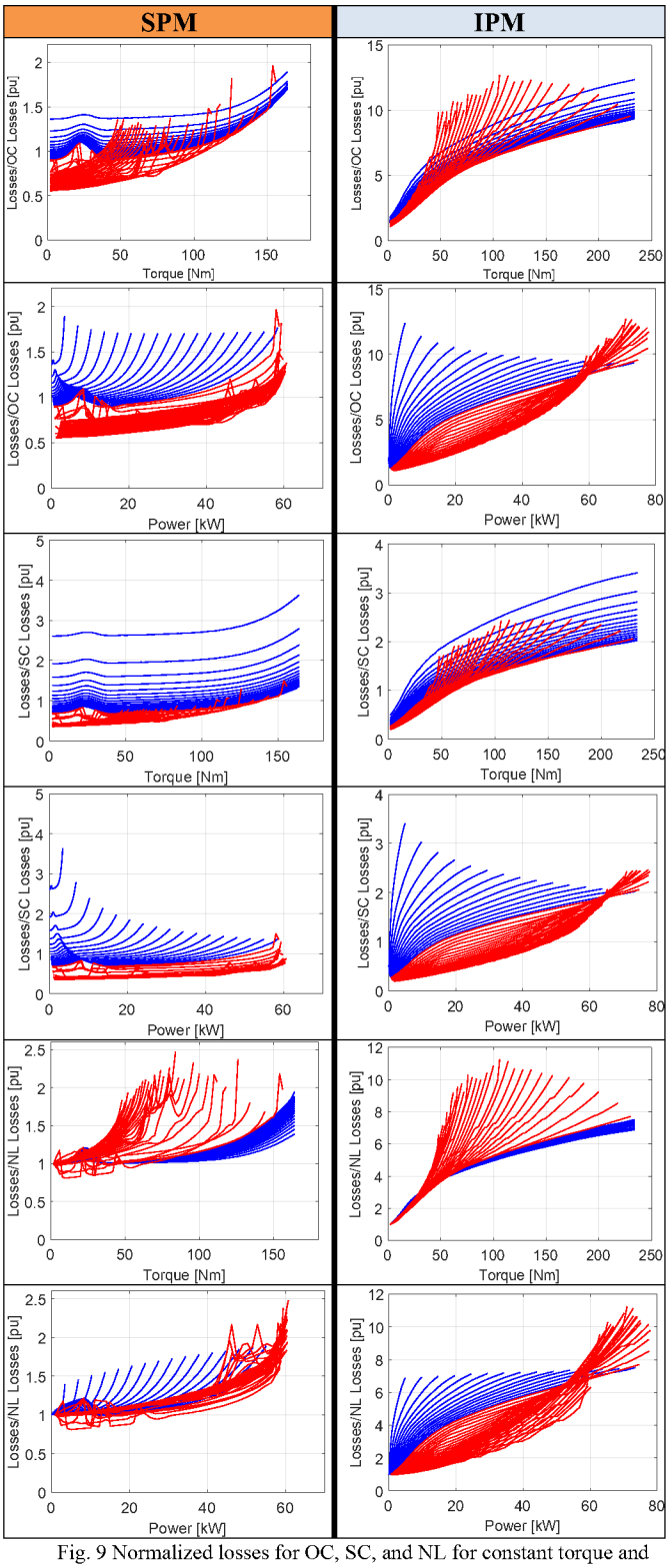

Fig. 9 Normalized losses for OC, SC, and NL for constant torque and constant power operation regions.

region for the SPM, in the T^2 and T^4 are used while for the IPM, $T^{1/2}$ and $T^{1/3}$ are compared. For the graphs with the best fit, e.g. T^4 for the SPM, a black line shows the linear function used for

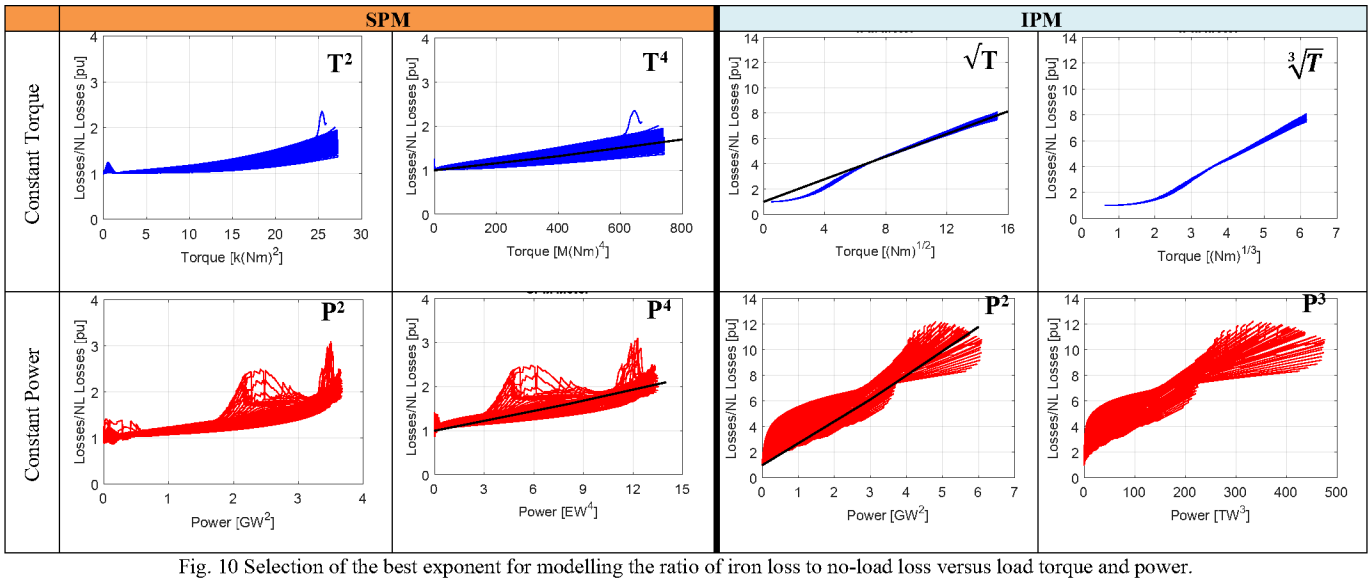

Fig. 10 Selection of the best exponent for modelling the ratio of iron loss to no-load loss versus load torque and power.

the fit.

Based on the above results, it was found that the iron loss at maximum efficiency can be estimated by scaling the NL loss $P_{fe\text{-}NL}(\omega)$ as a function of load torque T and power P as follows for the constant torque and power regions respectively,

$$P_{fe}(\mathrm{T},\omega) = P_{fe-NL}(\omega) \times K_T\left(\frac{T}{T_0}\right)^{n_T} \tag{8}$$

$$P_{fe}(\mathrm{P},\omega) = P_{fe-NL}(\omega) \times K_P\left(\frac{P}{P_0}\right)^{n_P} \tag{9}$$

where T_0 and P_0 are the rated torque and rated power, n_T and n_P the exponents for constant torque and constant power regions and K_T and K_p, the scaling factors representing the ratio of the full-load to no-load iron loss for each region. The values of the exponents and scaling factors are summarized in Table II.

The loss contour map obtained from the scaled-NL losses has been presented earlier in Fig. 6. Comparing these losses against the actual loss shown also in Fig. 6 illustrates a good correspondence between these results. The discontinuity in the contours in the scaled NL loss estimate at the rated speed is due to the use of different fitting functions in the constant torque and constant power regions.

Table III. Curve-Fit Parameters for No-Load Iron Loss.

	SPM		IPM	
	K	***n***	***K***	***n***
Constant Torque K_T, n_T	0.001	4	8	0.5
Constant Power K_P, n_P	0.075	4	0.002	2

D. Comparison of Exact and Estimated Efficiency Maps

Fig. 11 compares the exact efficiency map with the estimated efficiency maps using the saturation-only flux linkage model as well as iron loss model as only a function of speed based on the scaled no-load loss.

First consider the SPM. Case 1 shows the exact efficiency map. Case 2 shows that the saturation-only flux-linkage model over-estimates the low speed torque capability as this machine has a high degree of cross-saturation. Case 3 shows using the iron loss as only a function of speed introduces errors in the constant power regions which cause small changes particularly in the efficiency contours as they approach the capability limit. In this region, Case 4 shows significant improvement versus Case 3 and is much closer to Case 2 which uses the exact iron loss. Comparing Case 2 and 4 shows that the scaled-NL loss method predicted the efficiency map by maximum 1% error which only existed in the low torque region.

For the IPM, as the machine has a low level of cross-saturation, the effect of using the saturation-only flux-linkage model is negligible and thus the Case 2 and 1 results are similar. In Case 3, using the iron loss only as a function of speed significantly affects the accuracy of the values and shapes of the efficiency contours in the constant power region. Comparing Case 4 with Case 3 and 1, shows using the scaled NL loss produces a generally better efficiency map estimate in the constant power region though the peak efficiency is over-estimated by about 1%. Note that the use of different fitting functions in the constant torque and constant power regions produces a discontinuity in the efficiency contours at rated speed.

VII. Conclusions

This paper investigates estimating the efficiency map of an electric machine based on limited experimental test data. The results are validated using detailed finite-element data from 50-kW surface PM (SPM) and interior PM (IPM) machines. Two approximations are considered: modeling the flux-linkage by only considering saturation (not cross-saturation), and using iron loss data which is only a function of speed (not torque). These parameters are measured using simple experimental tests.

Errors in the flux-linkage modeling affect the estimation of the torque-speed capability envelope in the constant torque region and also the stator copper losses. It was found that the

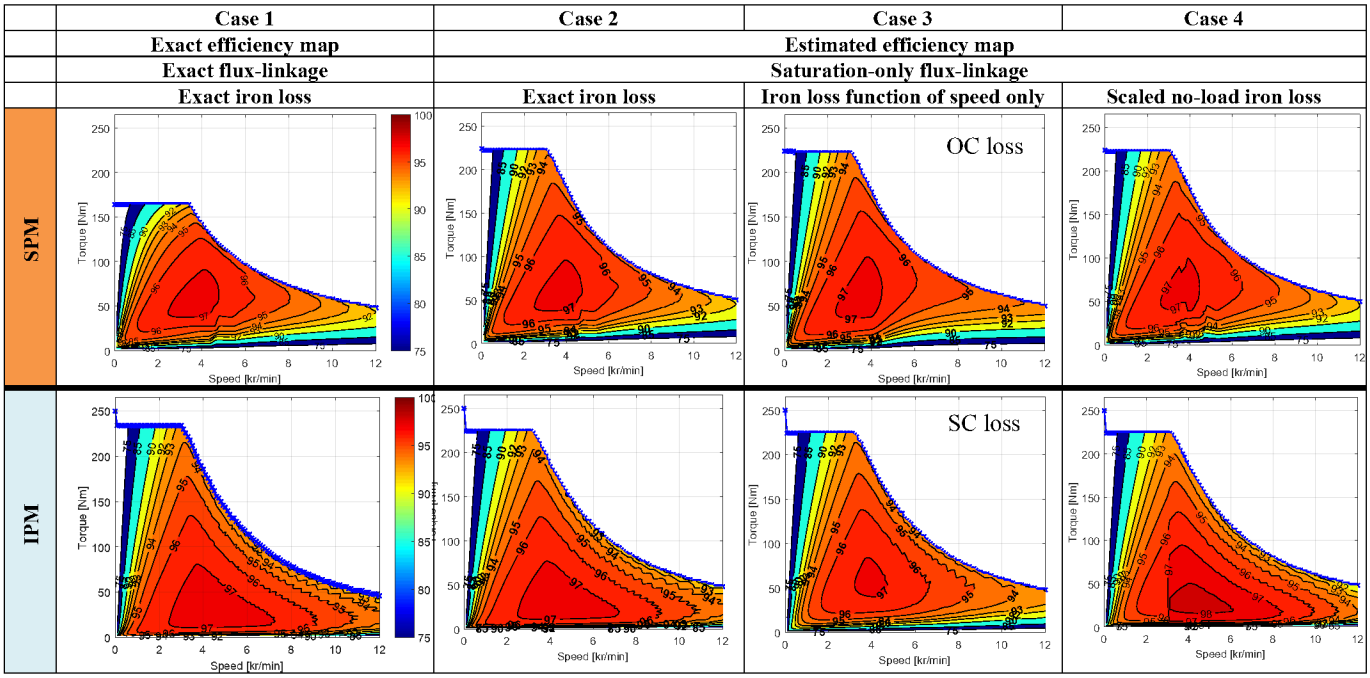

Fig. 11 Comparison of exact and estimated efficiency maps for SPM and IPM machines.

SPM machine had significant cross-saturation and thus showed substantial errors in the constant torque when using the saturation only model while the IPM had little cross-saturation and thus showed good results.

The iron loss at maximum efficiency is a function of both torque and speed. For simplicity, only iron loss data as a function of speed was considered (open-circuit, short-circuit and no-load). It was found that the open-circuit data gave the best approximation for the SPM machine and the short-circuit data for the IPM machine.

The paper investigated obtaining higher accuracy in the iron loss estimation by using the no-load loss data and modeling the increase in iron loss with load with an empirical function. It was shown that good results could be obtained using a power law function of torque in the constant torque region and a power law function of power in the constant power region. The best fit was obtained using significantly different scaling factors and exponents for the two machines. The scaled NL loss method predicted the efficiency map by a maximum of 1% error for both SPM and IPM machines.

VIII. REFERENCES

[1] A. Mahmoudi, W. Soong, G. Pellegrino, and E. Armando, "Loss Function Modeling of Efficiency Maps of Electrical Machines," *IEEE Transactions on Industry Applications,* 2017.

[2] A. Brune, P. Dück, B. Ponick, A. Kock, and M. Gröninger, "Evaluation of an efficiency-optimized calculation of PM synchronous machines' operating range using time-saving numerical and analytical coupling," in *Vehicle Power and Propulsion Conference (VPPC), 2012 IEEE*, 2012, pp. 32-35.

[3] S. Stipetic and J. Goss, "Calculation of efficiency maps using scalable saturated flux-linkage and loss model of a synchronous motor," in *Electrical Machines (ICEM), 2016 XXII International Conference on*, 2016, pp. 1380-1386.

[4] J. Goss, P. Mellor, R. Wrobel, D. Staton, and M. Popescu, "The design of AC permanent magnet motors for electric vehicles: A computationally efficient model of the operational envelope," 2012.

[5] S. Kahourzade, A. Mahmoudi, W. L. Soong, N. Ertugrul, and G. Pellegrino, "Estimation of PM Machine Efficiency Maps from Limited Experimental Data," in *2018 IEEE Energy Conversion Congress and Exposition (ECCE)*, 2018, pp. 4315-4322.

[6] A. Mahmoudi, W. L. Soong, G. Pellegrino, and E. Armando, "Efficiency maps of electrical machines," in *2015 IEEE Energy Conversion Congress and Exposition (ECCE)*, 2015, pp. 2791-2799.

[7] C. Lu, S. Ferrari, and G. Pellegrino, "Two design procedures for PM synchronous machines for electric powertrains," *IEEE Transactions on Transportation Electrification,* vol. 3, pp. 98-107, 2017.

[8] A. M. El-Refaie, T. M. Jahns, P. B. Reddy, and J. W. McKeever, "Modified vector control algorithm for increasing partial-load efficiency of fractional-slot concentrated-winding surface PM machines," *IEEE Transactions on Industry Applications,* vol. 44, pp. 1543-1551, 2008.